

Transient rheology of solvent-responsive complex fluids by integrating microrheology and microfluidics

Jun Sato and Victor Breedveld^{a)}

School of Chemical & Biomolecular Engineering, Georgia Institute of Technology, 311 Ferst Drive NW, Atlanta, Georgia 30332-0100

(Received 27 June 2005; final revision received 29 September 2005)

Synopsis

A new microrheology set-up which allows us to quantitatively measure the transient rheological properties of solvent-responsive complex fluids was constructed by integrating particle tracking microrheology and microfluidics. The dialysis cell consists of a reservoir, porous dialysis membrane, and sample chamber. Solvent molecules can freely diffuse between the reservoir and the sample chamber while macromolecular sample components are trapped in the sample chamber with a rigid semipermeable dialysis membrane. The design enables manipulation of the solvent composition in the sample chamber by simply switching the fluid composition in the reservoir. Validation experiments for solvent diffusion in the dialysis cell showed good agreement with numerical solutions of the transport equations and confirmed that the solvent composition in a sample can be changed in a controlled and predictable fashion within a few minutes due to the small device dimensions. For aqueous solutions of sodium alginate and sodium polystyrene sulfonate, transient rheological properties were measured in response to changes in salt concentration. The results showed that the dialysis cell is a useful and versatile tool to study the response of complex fluids to reversible changes in solvent composition. © 2006 The Society of Rheology. [DOI: 10.1122/1.2135329]

I. INTRODUCTION

Complex fluids are ubiquitous in nature, everyday life, and industry: foods, biological fluids, personal care products, electronic and optical materials, polymer melts and solutions [Larson (1999)]. Many of these materials contain solvent-sensitive components, for example, polyelectrolytes and surfactants, that enable control over the structure and flow properties. An example are stimuli-responsive hydrogels, which have attracted a lot of attention as functional materials due to their unique responses to external stimuli like *pH* and solvent composition. Such hydrogels have potential applications in the fields of drug delivery, tissue engineering, agriculture, cosmetics, gene therapy, and as sensors and actuators [Hoffman (1995); Peppas *et al.* (2000); Qiu and Park (2001); Gupta *et al.* (2002); Jeong and Gutowska (2002); Rudzinski *et al.* (2002); Soppimath *et al.* (2002); van der Linden *et al.* (2003)]. Understanding the responsiveness of the structure and rheology to environmental changes is essential for elucidation of gel formation mechanisms and the design of materials with desirable mechanical properties and functionality.

^{a)} Author to whom correspondence should be addressed; electronic mail: victor.breedveld@chbe.gatech.edu

In order to optimize the mechanical properties of solvent-responsive complex fluids, it is necessary to have the experimental ability to monitor rheological quantities during solvent changes. For traditional mechanical rheometry, a sample must be mixed homogeneously, loaded into a rheometer, and rested before a measurement can be performed. As a result, only samples with slow dynamics can be investigated: the rheological properties must remain unchanged during sample preparation and loading. It is challenging to manipulate the pH or salt concentration in a sample after loading, and therefore it is virtually impossible to measure the rheological response to controlled changes in solvent composition in a rheometer. For example, Goeden-Wood *et al.* recently attached a dialysis membrane around a cone-and-plate geometry to induce pH -buffer exchange [Goeden-Wood *et al.* (2003)] during the preparation of solvent-sensitive peptide solutions. The authors waited for 12 h to achieve equilibrium; the long waiting time was due to the large distance over which diffusive transport had to occur (12.5 mm, the cone radius) and thus it was impossible to resolve transient rheological changes in the sample. As a result of such experimental limitations, solvent composition has not been treated as control parameter for the rheology of complex fluids as extensively as other environmental conditions like mechanical stress, temperature, UV-light, and electromagnetic fields.

Instead of measuring the full mechanical properties, the volumetric response (swelling) of thin polymer gel films (0.1–1 mm) to external stimuli has been researched extensively [Brannonpeppas and Peppas (1990); (1991); Siegel *et al.* (1992); Hassan *et al.* (1997); Kim *et al.* (2003)]. Experiments are typically carried out by immersing a sample directly into solvent and monitoring its volume or weight; this method can only be applied to highly cross-linked gels. In other work, photolithography has been used to create samples with a short diffusion path (200–400 nm) inside microfluidic devices (thickness $\sim 50\ \mu\text{m}$) to investigate the time-dependent expansion of hydrogels [Chen *et al.* (1998); Beebe *et al.* (2000)]. This approach is limited to photopolymerizable polymers and shape changes are measured rather than mechanical properties. Similar perfusion chambers are common in cell physiology, tissue engineering, and biochemistry; solvents are flowed past tissue slices or cells and their response is monitored. Because the samples experience external shear stress in perfusion chambers, cells typically must be tethered inside the sample chamber.

Although the studies listed above did not succeed in measuring time-dependent mechanical properties of complex fluids, some lessons can be learned from this work. Diffusion through a dialysis membrane is an excellent method for solvent manipulation in macromolecular fluids, but samples must be thin. Moreover, the membrane must be selective: permeable to solvent molecules, but not to the macromolecular components of interest. To minimize the hydrodynamic stress that cells experience in a perfusion chamber, McGrath *et al.* (1985); (1986); (1997) constructed a diffusion chamber for an optical microscope to study the osmotic response of cells to solvent exchange [McGrath (1985)]. Cells were entrapped inside a thin cell compartment ($\sim 100\ \mu\text{m}$), which was sealed off with a thin dialysis membrane ($\sim 16\ \mu\text{m}$). Rapid exchange could be achieved through diffusion from the external flow side of the chamber to the cell compartment. Transient concentration histories in the cell compartment were measured with electroconductivity [Porsche *et al.* (1986)], and controlled with a computer, although a detailed description has not been published [McGrath and Krings (1986)]. The authors successfully monitored the dynamic osmotic response of individual cells with microscopy, but did not measure mechanical properties during the solvent changes. Several experimental problems were reported [McGrath (1997)]: fragility of the membrane, introduction of air bubbles, and mobility of cells inside the cell compartment.

With a similar device, Hou *et al.* (1990) studied the transient copolymerization process

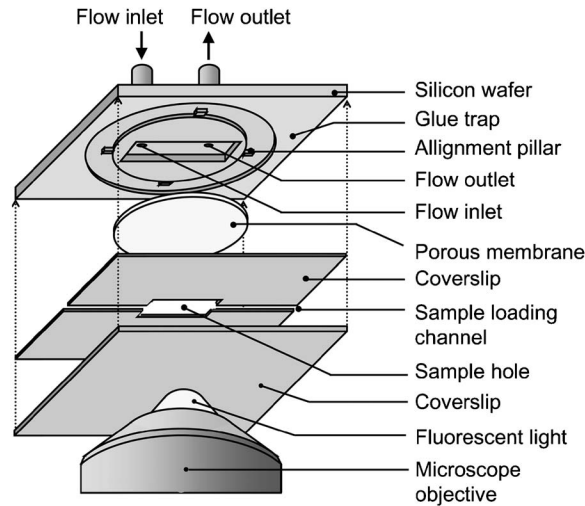


FIG. 1. Schematic representation of the dialysis cell.

of F-actin and filamin [Hou *et al.* (1990)]. In addition to direct visualization of the growing actin network, the Brownian motion of premixed tracer particles was used to qualitatively monitor structural changes of the polymer network. However, in these experiments the time scales of the diffusion process were not precisely determined, and significant lag times were observed, most likely due to Taylor dispersion in the inlet tubing. Quantitative rheological characterization of the polymerization process was not performed.

For measuring rheology in small sample volumes, particle-tracking microrheology has become a well-established noninvasive method [Mason and Weitz (1995); Mason *et al.* (1997)]. Microrheology requires only a small sample size ($\sim \mu\text{l}$) for rheological measurements, much less than conventional mechanical rheometers, which require at least hundreds of μl . Microfluidic techniques enable the construction of small-scale sample geometries in which particle-tracking microrheology can be performed [Stone and Kim (2001)]. The goal of our work was to construct a novel microrheology set-up for measuring the transient rheological properties of complex fluids in response to solvent change by combining particle tracking microrheology and microfluidics in a dialysis cell for microrheology.

II. DIALYSIS CELL

A. General idea

Conceptually, the dialysis cell is based on a three-layer geometry: a reservoir channel that is connected to an external flow loop, a rigid porous membrane, and a sample chamber of constant volume. The entire system must be configured so that it can be mounted on an inverted microscope to enable particle tracking microrheology as shown in Fig. 1. The solvent composition in the reservoir can then simply be controlled by manipulating the fluid flow. Solvent molecules in the reservoir can diffuse freely in and out of the sample through the porous membrane. Large molecules within the sample chamber cannot diffuse out, provided that the membrane has the appropriate size-selectivity.

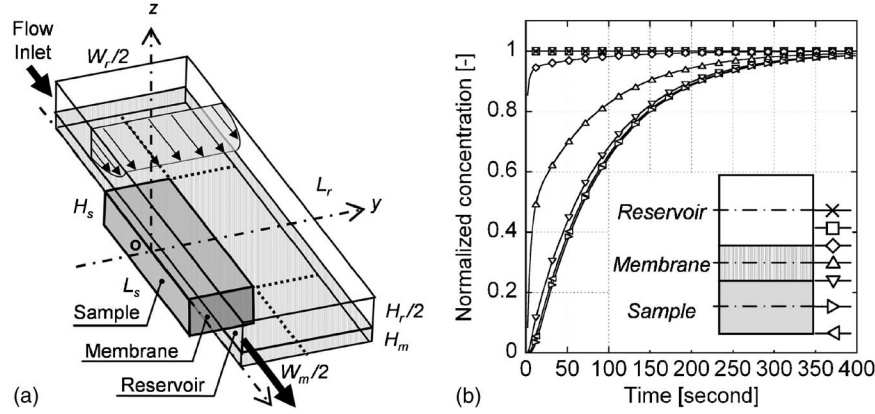


FIG. 2. (a) Three-dimensional geometry of the dialysis cell (only one half shown for clarity): $H_r=200\ \mu\text{m}$, $H_m=60\ \mu\text{m}$, $H_s=120\ \mu\text{m}$, $L_r=1\ \text{cm}$, $L_s=5\ \text{mm}$, $W_r=3\ \text{mm}$, $W_m=1.5\ \text{mm}$. A sketch of the velocity profiles in the reservoir is also included. (b) Time-dependent concentration profiles of Ca^{2+} ions, calculated with a finite volume method at: reservoir centerline (\times), halfway between reservoir centerline and bottom (\square), reservoir bottom (\diamond), membrane center (\triangle), sample top (∇), sample center (\triangleright), and sample bottom (\triangleleft) (see inset). Pressure gradient is $-3810\ \text{Pa m}^{-1}$ and viscosity is $1\ \text{mPa s}$. $D_0=7.92 \times 10^{-10}\ \text{m}^2\ \text{s}^{-1}$, $G=0.15$, $H=0.88$, and $x_{\text{test}}=5000\ \mu\text{m}$.

If the dimensions of the device are chosen appropriately, diffusive transport can be considered one-dimensional and the characteristic diffusion time, t_D , is a function of sample thickness, d , and diffusion coefficient, D , of the diffusing agent: $t_D=d^2/2D$. This simple scaling argument shows that constructing a system with small sample dimensions is crucial. The characteristic diffusion time of several hours that was observed for a 25 mm diameter cone-and-plate geometry [Goeden-Wood *et al.* (2003)] should decrease to a few seconds for a sample thickness of 0.10 mm.

Rapid and reversible changes of sample solvent composition can be achieved by switching the external flow through a supply system of syringe pumps, tubing and valves, provided that transport limitations in the flow loop (e.g., Taylor dispersion) are eliminated. Fluorescent tracer particles can be premixed with the sample to enable rheological measurements throughout a solvent-exchange experiment via particle tracking microrheology. The transient rheological response of a sample can thus be measured with high temporal resolution.

B. Numerical calculation

The transient concentration profiles in the dialysis cell were calculated numerically to characterize the mass transport, and to determine dimensions and flow conditions that would lead to the desired responsiveness of the dialysis cell. For a similar device, McGrath obtained numerical results that indicated that membrane diffusion was the rate-limiting process, but detailed results have not been published.

The three-dimensional geometry of the dialysis cell is shown in Fig. 2(a) which depicts only half of the cell for clarity. The cross-sectional aspect ratio, W_r/H_r , in the reservoir is 15. As illustrated in the sketch, the velocity profile in the y -direction is pluglike while the profile in the z -direction is parabolic [Gondret *et al.* (1997)]. The sample chamber is narrower than the reservoir and aligned with the center of the reservoir, so that the velocity profile is nearly independent of y in the contact area with the

sample. As a result, one can ignore velocity gradients in the y -direction at high Peclet number conditions ($Pe = W_r \cdot v_x / D$, v_x being the velocity in the x -direction) and assume two-dimensional mass transport.

Since transport in the device involves both diffusion and convection, a finite volume method (FVM) was used to eliminate numerical diffusion in solving the convection-diffusion equation by using a finite volume discretization formulation [Patankar (1980)]. Key assumptions used for the calculation are: (1) transport is two-dimensional and no diffusion occurs in the y -direction, and (2) homogeneous concentration changes occur at the reservoir inlet immediately after switching the solvent composition, thereby neglecting the effect of Taylor dispersion in the tubing between switching valve and reservoir inlet. Appropriate mesh sizes and timesteps were chosen for the calculation. Flow conditions were set to achieve a realistic average velocity in the reservoir of 1.25×10^{-2} m/s [Gondret *et al.* (1997)]. The diffusion coefficient used in the calculations was 7.92×10^{-10} m² s⁻¹, the literature value for Ca²⁺ at infinite dilution [Lide (2003)].

For hindered diffusion of solute through liquid-filled pores, the effective diffusion coefficient in the membrane can be written as [Hines and Maddox (1984); Deen (1987)],

$$D_{\text{membrane}} = H \cdot \frac{\varepsilon}{\tau} \cdot D_0 \equiv H \cdot G \cdot D_0. \quad (1)$$

D_{membrane} and D_0 are the effective diffusivity and the diffusivity of solute at infinite dilution. ε , τ , and H are, respectively, the membrane porosity, tortuosity, and hindrance factor due to the finite pore sizes. H is a function of the ratio of solute diameter, d_s , to pore diameter, d_p : $\lambda = d_s/d_p$; H becomes 1 when $\lambda = 0$. ε and τ are geometrical factors, so that $G (= \varepsilon/\tau)$ should be determined only by the membrane structure and be constant for the specific membrane. For the calculations presented in this section, we used $G = 0.15$ (see Sec. III for the origin of this value) which is equivalent to an effective diffusion coefficient of 1.1×10^{-10} m² s⁻¹ for calcium ions. In this study, our samples consist of polymer solutions in deionized water at <1 wt. % of polymer. Therefore, the D_0 in the sample layer is assumed to be the same as D_0 in deionized water. For alginate gels, this assumption was confirmed by Tanaka *et al.* (1984).

Time-dependent concentration profiles at $x = 2.5$ mm (the middle of the sample chamber) are shown in Fig. 2(b) for seven different z -locations: the centerline of the reservoir; the midpoint between the centerline of the reservoir and the membrane; the bottom of the reservoir; the middle of the membrane; and the top, middle and bottom of the sample layer (see legend). After the concentration at the reservoir inlet was changed in a stepwise manner, the concentrations across the reservoir responded rapidly; the final concentration at the centerline of the reservoir is reached within a few seconds. A noticeable delay was observed at the top surface of the membrane, which results from slow convective transport in the proximity of the membrane. The concentration response on the sample side of the membrane is much slower. There is not a significant difference between the concentration curves at different locations in the sample chamber, which proves that transport through the membrane is the rate-limiting process, in agreement with literature [McGrath (1985)]. The concentrations in the sample chamber reach about 50% of the inlet concentration after 1 min, 90% after a few minutes, and asymptotically approach the inlet concentration.

C. Microfabrication

Photolithographical techniques were employed to construct the dialysis cell. The dialysis cell was constructed from three elements: a top part, the membrane and a bottom

part (Fig. 1). The top part has four distinct features: a rectangular reservoir channel, circular membrane insert, a trench for application of adhesives, and holes for flow inlet/outlet. The bottom part consists of a glass coverslip with a rectangular hole to serve as sample chamber, and a second coverslip that seals the sample and enables optical access on an inverted microscope.

The top structure was etched in silicon wafer (475–575 μm thick, NOVA Electronic Materials, Ltd). Chrome photomasks were manufactured on borofloat substrate (1.1 mm thick, TELIC Co., Ltd). A positive photoresist (4620, Clariant Co.) was spin-coated ($\sim 15\ \mu\text{m}$ thick) on the silicon wafer and softbaked on a hotplate (CEE 100CB, Brewerscience, Inc.). The wafer was then exposed to UV-light (2000 mW/cm^2 , OAI Mask Alignment and UV Exposure System, Optical Associates, Inc) and immersed in an AZ400K developer 1:4 (Clariant Co.) for several minutes to finish patterning. Features were then fabricated with plasma etching (Dual ICP SLR Mn F. Model, Plasma Therm Inc.) and the dry etching was completed by rinsing the photoresist. The fabrication process was repeated with different masks in the following order: (1) the trench for application of adhesives, (2) the circular membrane insert, (3) the reservoir channel, and (4) the inlet/outlet holes. As a dialysis membrane, AnodiscTM aluminum oxide membranes were selected because of their small thickness and high rigidity (13 mm diameter, 60 μm thick, 20 nm nominal pore diameter, 25%–30% porosity; Whatman International Ltd.).

Figure 1 illustrates how the dialysis cell was assembled. The circular membrane fits in the insert and is aligned with four pillars. A diamond cutter was used to cut the rectangular hole for the sample chamber ($5 \times 1.5\ \text{mm}$) in a No. 0 cover slip, which was then split into half. The two pieces were placed onto the silicon wafer and membrane with a small separation, thus forming a narrow channel for sample loading. Capillary forces are responsible for filling all cracks with UV-glue (B-690-0, Bohle), which was then cured through exposure to UV light. Subsequently, the second cover slip (No. 1.5) was placed onto the assembly and fixed with UV glue as well. Thermally curable adhesive (N-100-01, Upchurch Scientific) was used to attach connectors (N-333, Upchurch Scientific) to the flow inlet/outlet ports of the dialysis cell.

Before sample loading, the inlet and outlet ports of the reservoir were connected to flexible tubing filled with solvent. By adjusting the relative vertical position of the membrane and the tubing, the effects of hydrostatic pressure were minimized to eliminate pressure-driven transport between sample and reservoir and facilitate sample loading. The sample chamber has a volume of approximately $0.9\ \mu\text{l}$ and can be filled with a pipette. Even highly viscous or viscoelastic samples can be loaded into the device by placing the sample at one end of the channel and creating underpressure at the other end to suck the sample into the chamber. After loading the sample, quick-dry nail polish was used to seal both ends of the channel. In some cases (i.e., polyelectrolyte solutions with high osmotic pressure), polymer adhesive melts were used to reinforce the seal. The dialysis cell makes it possible to load a sample quickly and confine it to the sample chamber of constant volume without leakage.

D. Flow system

An aluminum foundation was designed to mount the dialysis cell and tubing on a Leica DM-IRB inverted microscope, which is placed on an air table to dampen external vibrations. The flow system is shown in Fig. 3. Two syringes were connected to a syringe pump (KDS210C, KD Scientific Inc.) and a four-port switching valve (V-101D, Upchurch Scientific) was placed in the tubing upstream of the dialysis cell. Both syringes were connected to the inlet ports of the valve. One of the outlet ports led to the reservoir

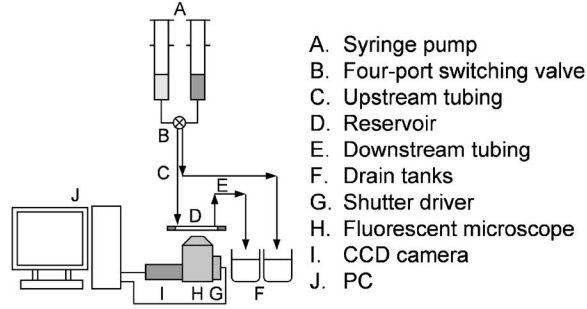


FIG. 3. Flow system and measuring system.

channel and then emptied into a drain tank, while the other outlet led directly to the drain tank. This set-up enables rapid switching between two source fluids during continuous operation of the syringe pump. In order to minimize the dead volume between valve and dialysis cell, and thus the response time of the system, fine tubing (0.25 mm diameter, PEEK™, Upchurch Scientific) was used to connect the valve and dialysis cell. Larger tubing (1 mm diameter, PEEK™, Upchurch Scientific) was used between reservoir outlet and drain tank to minimize pressure drops. The flow rate can readily be measured by monitoring the weight of the drain tank with an analytical balance.

E. Video microscopy and microrheology

The microscope was equipped with an analog 640×480 pixel CCD camera (30 Hz frame rate, COHU 4920, Poway, CA), which was connected to a PC. Images were transferred to the PC and recorded real-time with a precision frame grabber (PXC-200, Cyber Optics) and specialized image acquisition software (OpenBox) [Keller *et al.* (2001)]. A high-speed shutter (Uniblitz® VMM-D1, Vincent Associates Inc.) was inserted in the microscope fluorescent light path, so that illumination could be controlled via a LabView interface. The resolution with $63\times$ and $100\times$ objectives was $0.157 \mu\text{m}$ per pixel and $0.099 \mu\text{m}$ per pixel, respectively. Fluorescent probe particles were selected so that their surface chemistry was compatible with sample properties: negatively charged carboxylate-modified or positively charged amine-modified polystyrene particles of various sizes ($0.37\text{--}2 \mu\text{m}$ diameter, Molecular Probes Co.). The probe particles were premixed in the samples, so that rheological properties could be measured by carrying out particle tracking microrheology [Mason and Weitz (1995); Mason, *et al.* (1997); Breedveld and Pine (2003)] according to the scheme outlined in Fig. 4.

Particle tracking microrheology takes advantage of a generalized Stokes-Einstein relation,

$$\langle \Delta \tilde{r}^2(s) \rangle = \frac{dk_B T}{3\pi a s \tilde{G}(s)}, \quad (2)$$

where $\langle \Delta \tilde{r}^2(s) \rangle$ is the Laplace transform of the mean-squared-displacement (MSD) $\langle \Delta r^2(\tau) \rangle$, τ is the lag time, s is the Laplace frequency, a is the radius of the tracer particles, k_B is Boltzmann's constant, T is the absolute temperature, and d is the dimensionality of the displacement vector Δr . In our experiments, particle positions and trajectories were detected through image analysis with the software package IDL (Research Systems Inc.), using algorithms developed by Crocker and co-workers [Crocker and Grier (1996)]. The MSD was calculated based on these trajectories. Equation (2) can then

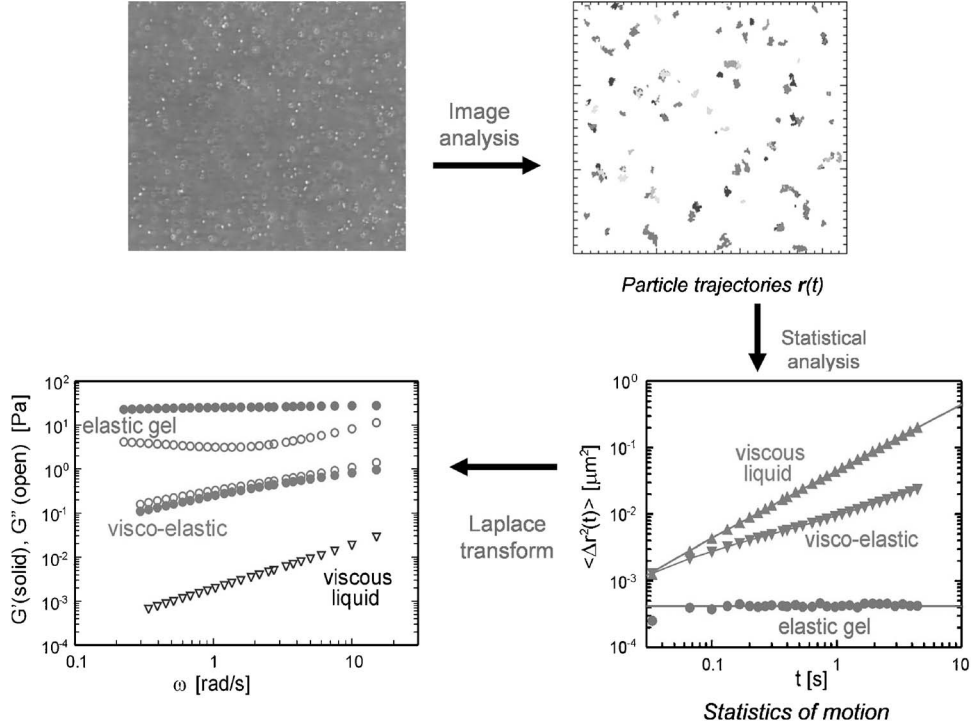


FIG. 4. Diagram of microrheology system.

be used to find $\tilde{G}(s)$ and the complex shear modulus: $G^*(\omega) = G'(\omega) + iG''(\omega)$ by substituting $i\omega$ for the Laplace frequency s [Mason (2000)]. For viscous liquids, the slope of MSD vs τ in a double-logarithmic plot is 1, while for elastic gels, MSD reaches a plateau with increasing lag time.

In standard microrheology experiments, it is generally assumed that the rheological properties do not change during the image acquisition and the MSD is averaged over the entire length of the movie. In transient experiments with the dialysis cell, however, the MSD must be determined as a function of both the lag time τ and the clock time, t . This is achieved by cutting the initial trajectories into segments of duration Δt and calculating MSD as the average over the time interval from $t - \frac{1}{2}\Delta t$ to $t + \frac{1}{2}\Delta t$,

$$\langle \Delta r^2(\tau, t, \Delta t) \rangle = \langle \Delta r^2(\tau) \rangle_{(t - \frac{1}{2}\Delta t, t + \frac{1}{2}\Delta t)}. \quad (3)$$

By following this strategy, we can monitor the rheological response of a sample to solvent composition changes. The interval length Δt must be chosen with two primary concerns in mind: statistical validity and temporal resolution. To minimize statistical errors, Eq. (3) must satisfy the condition: $\Delta t \gg \tau_{\max}$, where τ_{\max} is the maximum lag time at which the MSD is to be determined. If Δt is of the same magnitude as τ_{\max} , $\langle \Delta r^2(\tau_{\max}) \rangle$ involves significant statistical errors because of averaging over a small number of independent data points Δr within the interval Δt . On the other hand, a large value of Δt leads to poor temporal resolution and reduces the experimental ability to accurately capture physical transitions in a sample. To balance these requirements, we generally limit the range of our lag times by choosing relatively small values of τ_{\max} . To ensure statistical validity, all MSD values were calculated by taking the ensemble average of at least 1000

independent contributions [Breedveld and Pine (2003)]. For highly viscous or elastic samples, MSD values at short lag times τ can be very small, and sometimes be close to the spatial detection limit. In preliminary investigations (not reported here), the spatial resolution of the experimental set-up used in this study was measured by embedding particles in highly elastic gels; the minimum attainable MSD was $\sim 2 \times 10^{-5} \mu\text{m}^2$, which corresponds to tracer displacements of 4–5 nm. In the current study Δt was varied from 1.3 to 2.6 s (40–80 video frames), which is small enough to accurately capture the physical transitions in our samples (see Figs. 7–9).

III. VALIDATION TEST: FLUORESC EIN SOLUTION

After fabrication, the performance of the dialysis cell was validated by comparing experimental transient concentration curves to the results obtained from numerical calculations (Sec. II B). In these validation experiments, we used fluorescein (F-6377 Sigma) which has a molecular size that is small enough to diffuse freely through the membrane pores, and a known diffusion coefficient of $5.2 \times 10^{-10} \text{ m}^2 \text{ s}^{-1}$ [deBeer *et al.* (1997)]. Also, the concentration of aqueous fluorescein solutions can be measured with digital video-microscopy by constructing a calibration curve between image brightness and fluorescein concentration. With our 8-bit CCD camera, image brightness is quantified digitally in the range between 0 and 255 and in order to obtain good experimental resolution, the brightness needs to cover a wide dynamic range. Taking this into account, the concentrations of the fluorescein samples for the calibration curve were chosen between 0.01 mM and 0.075 mM. A $100\times$ oil immersion objective was used to minimize the depth of focus and background fluorescence. Any remaining background signal due to fluorescein in the reservoir could clearly be identified and subtracted from the measured transient brightness.

To minimize the effect of photobleaching on the transient concentration curves, experiments were performed using brief (70 ms) exposures of the sample to fluorescent light, followed by longer dark intervals. For the 0.075 mM fluorescein solution, experiments were carried out with dark interval lengths of 2, 6, 10, and 14 s. The excellent agreement between all curves (not shown here) proved that experimental parameters sufficiently eliminated photobleaching effects. To further validate our results, we used confocal scanning laser microscopy (CSLM) (VT-eye, VisiTech International) for a single control experiment. CSLM has been widely used for measuring the local diffusion coefficient of fluorescent dyes [deBeer *et al.* (1997)] and has the distinct advantage that background brightness is minimized due to an extremely small depth of focus. The CSLM results agreed very well with fluorescence microscopy experiments, providing final proof that fluorescence microscopy can be used for quantitative measurements of fluorescein concentrations. To maximize temporal resolution, we then used 70 ms exposure intervals and 2 s dark intervals for subsequent validation experiments.

The equilibrium brightness at different fluorescein concentrations was measured 16 min after switching the reservoir flow from DI-water to fluorescein solution and used to construct the calibration curve between concentration and brightness [inset of Fig. 5(b)]. The calibration curve was linear over the entire range of concentrations, so that brightness data could easily be converted to concentrations and normalized by the known inlet concentration.

Next, the fluorescein concentration was changed in a stepwise fashion from low concentration to high concentration as listed in Table I. This approach was chosen to eliminate potential effects of adsorption of fluorescein molecules on the membrane surface. The membrane pretreatment was performed for 15 min before the image acquisition was

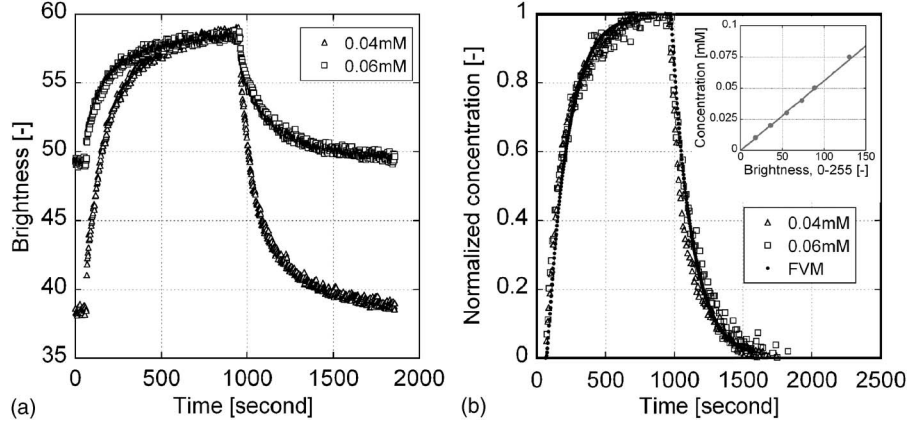


FIG. 5. (a) Transient brightness for two different fluorescein concentrations. (b) Normalized concentration curves and results of numerical calculations with $D_0=5.2 \times 10^{-10} \text{ m}^2 \text{ s}^{-1}$, $G=0.15$, and $H=0.82$. Calibration curve for fluorescein is depicted in the inset.


started. The reservoir flow was switched to higher fluorescein concentrations after 1 min and back to the initial concentration after 16 min. The experiments were repeated with different initial concentrations (0.04 mM and 0.06 mM) and a fixed final concentration (0.075 mM). Brightness was measured throughout the experiments [Fig. 5(a)] and converted to normalized concentration curves following the method described above [Fig. 5(b)].

If the porosity and tortuosity of the membrane are precisely known and the membrane structure is simple, one can calculate G directly from these geometry parameters [Eq. (1)]. However, Anopore membranes have a complicated treelike structure which contains a number of branches, curves and tapers with a wide pore size distribution [Hernandez *et al.* (1995); Bowen *et al.* (1996); Hernandez *et al.* (1997); Moaddeb and Koros (1997)] and the reported porosity values depend on experimental method [Palacio *et al.* (1999)]. Therefore, we used G as a fitting parameter to match experimental and numerical results. The calculations were iterated with different values of D_{membrane} until the results fitted the experimental data [Fig. 5(b)]. The hindrance factor H was calculated as 0.83, based on the hydrodynamic radius of fluorescein $\sim 0.45 \text{ nm}$ [Montermini *et al.* (2002)] and nominal pore size of 200 \AA . With the obtained D_{membrane} , G was then calculated to be 0.15 [Eq.

TABLE I. Composition of the reservoir flow during validation experiments with fluorescein solutions. Fluorescein concentrations were varied.

Switching time	Interval (min)	Reservoir flow
	15	Surface pretreatment
0	1	Low fluorescein concentration
1	15	High fluorescein concentration
16	15	Low fluorescein concentration
31		

TABLE II. Composition of the reservoir flow during sodium alginate experiment. CaCl_2 concentration was varied.

Switching time		Interval (min)	Reservoir flow
0		1	150 mM NaCl
1		5	CaCl_2
6		5	75 mM sodium citrate
11		5	
16		5	

(1)]. This geometrical factor is a material constant for the membrane. In the subsequent experiments, $G=0.15$ was used to estimate effective diffusion coefficients D_{membrane} for other solutes, such as Ca^{2+} and Na^+ .

IV. TRANSIENT RHEOLOGY

After design and construction of the dialysis cell and validation of its transport properties, the device was applied to study two materials with interesting rheological behavior: aqueous solutions of sodium alginate and sodium polystyrene sulfonate (NaPSS). The rheological properties of both materials can be changed dramatically by manipulating the solvent composition: liquid-to-gel-to-liquid transitions for sodium alginate and viscosity changes for NaPSS. The goal was to monitor the transient microrheology during solvent exchanges and demonstrate the applicability of the dialysis cell for different systems.

A. Sodium alginate

Sodium alginate is a polysaccharide that consists of two different monomers: 1,4-linked β -D-mannuronic and α -L-guluronic acid. In solution, it can form a gel by crosslinking with divalent cations like Ca^{2+} [Wang *et al.* (1991); (1994)] through the formation of a so-called “egg box” structure [Grant *et al.* (1973); Matsumoto and Mashiko (1990)]. The gel breaks up upon addition of chelating agents, e.g., sodium citrate, which form complexes with multivalent cations and thus extract Ca^{2+} from the gel [Shirai *et al.* (1987); Smidsrod and Skjakbraek (1990)].

For sample preparation, 1 g stock solution of 1.0 wt. % sodium alginate in 150 mM NaCl (Keltone LVCR®, ICP) was prepared, mixed on a vortex mixer, and left over night. Subsequently, 25 mg of this stock solution was mixed with 150 mM NaCl solution and carboxylate modified fluorescent particles (F8819, 1.0 μm diameter, Molecular Probes). The tracer particles were dispersed homogeneously throughout the sample and the final alginate concentration was adjusted to be 0.25 wt. %.

The solvent composition in the sodium alginate sample was changed according to the program listed in Table II. The reservoir flow started with 150 mM NaCl. After 1 min, the reservoir flow was switched to a CaCl_2 solution, after which Ca^{2+} ions could freely diffuse into the sample chamber filled with the aqueous sodium alginate solution. Then, the reservoir fluid was changed to a solution of chelating agent, 75 mM sodium citrate, which can diffuse through the membrane pores as well. Finally, the CaCl_2 solution was applied again. The experiment was performed with different CaCl_2 concentrations ranging from 0.028 wt. % to 1.11 wt. %.

In order to benchmark the microrheological measurements, the particle mean-squared displacement was first determined in the dialysis cell at steady state before and after gel

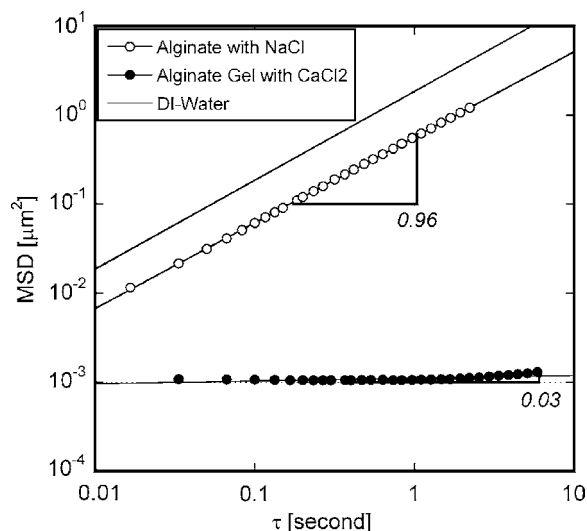


FIG. 6. MSD vs τ . (○) before gel formation and (●) after gel formation for 0.25 wt. % alginate solution in 150 mM NaCl and 0.111 wt. % CaCl_2 .

formation; the MSD vs τ curves are shown in Fig. 6. Note that τ can be large for these steady state experiments, since there are no temporal resolution limitations [Eq. (3)]. The slope in the double-logarithmic plot of the MSD curve before gel formation was 0.962, which indicates that tracer particles exhibited free diffusion and the sample behaved like a Newtonian liquid. The corresponding viscosity was calculated to be 2.94 mPa s. After exposure to Ca^{2+} , the slope of the MSD curve decreased dramatically and became 0.031, the signature of a highly elastic gel.

To confirm the accuracy of microrheological experiments, a direct comparison with macrorheology was made. A stock solution (1.0 wt. % sodium alginate, 600 mM NaCl) was prepared in a vial and mixed on a vortex mixer. After leaving the sample for 48 h, the stock solution was diluted with DI-water and fluorescent probe particles were added, so that a 0.25 wt. % Alginate solution in 150 mM NaCl was obtained. Samples were loaded between a microscope slide and a coverslip, using paraffin film as spacer and tightly sealing the sample holder with vacuum grease. The viscosity for the sample was 2.47 mPa s. For the same sample, viscosity measurements were also performed on a controlled stress rheometer (MCR300, Anton Paar) with a cone-and-plate geometry (50 mm diameter, 1° angle). The measured viscosity was 2.57 mPa s, which is in good agreement with the microrheology results for the sample. The deviation from the transient microrheology results in the dialysis cell listed above must originate from differences in sample preparation history. In the dialysis cell, samples are dialyzed continuously, while the experiments in a closed sample cell do not enable ion-exchange processes. From the direct comparison with rheometer measurements, we conclude that microrheology quantitatively measures the bulk rheological properties of alginate solutions.

In transient experiments, the slope of MSD vs τ must be determined for short lag times τ , much shorter than the time scale of physical property changes [Fig. 7(a)]. The three curves in Fig. 7(a) represents the transient behavior of MSD at lag times $\tau=0.033$, 0.067, and 0.1 s, which correspond to the dotted lines in the inset. The results in Fig. 7(a) show excellent recovery of viscous properties after inducing gel break-up with sodium citrate. If alginate molecules had diffused out from the sample chamber during the measurement,

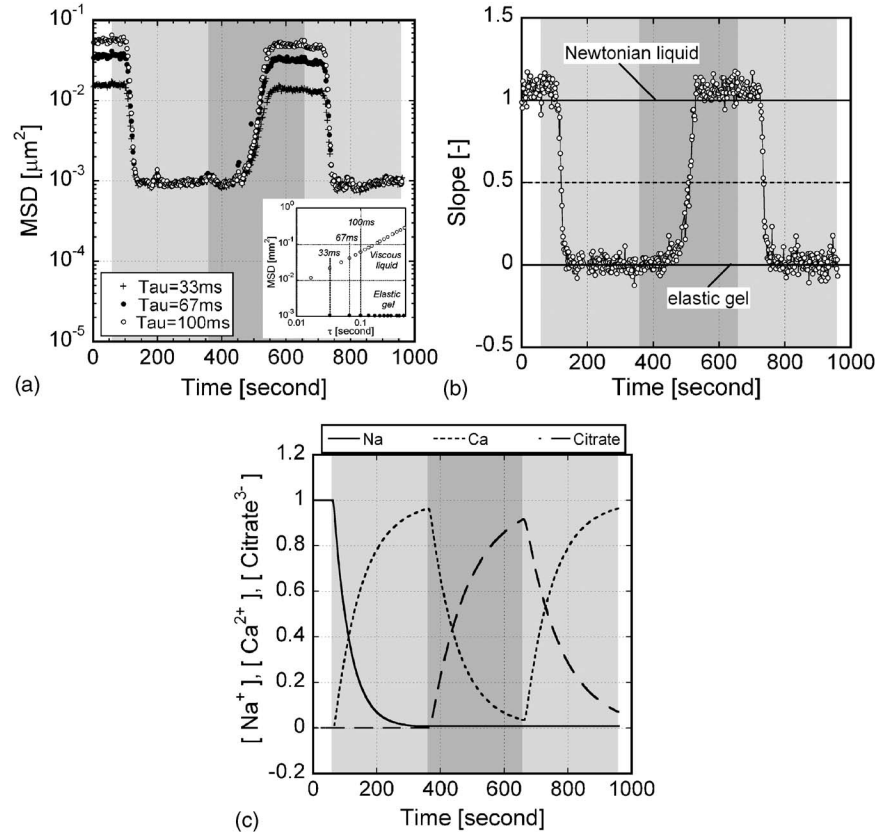


FIG. 7. (a) The transient MSD: τ =(+)33 ms, (●) 67 ms, and (○) 100 ms, solvents: (□) NaCl, (light shaded area) CaCl_2 , and (dark shaded area) sodium citrate. The steady state MSD curves are depicted in the inset and the dotted lines represent τ =33, 67, and 100 ms. (b) The transient slope $[\log(\text{MSD}) \text{ vs } \log(\tau)]$. (c) Numerical calculations of normalized solvent composition.

the alginate concentration and viscosity would have decreased and thus the MSD would have increased. The absence of such effects proves the selectivity of the dialysis membrane for the alginate solution. Upon gel formation and breakup, nondiffusive convective motion of the tracer particles was observed. This is the result of macroscopic gel shrinkage and swelling, which is commonly observed during formation of polymer gels. The effect of the convective motion on the calculated MSDs was eliminated by subtracting the average motion from the individual particle trajectories.

By applying a linear curve fit to the double-logarithmic plot of MSD vs τ , the slope of the double-logarithmic plot was obtained as a function of time [Fig. 7(b)]. Initially, the slope was equal to 1 in the presence of NaCl and decreased to 0 after the addition of CaCl_2 . By adding sodium citrate, the slope increased again and recovered its initial value of 1. After switching to CaCl_2 for a second time, the slope decreased once again to 0. This can directly be interpreted as a sequence of liquid \rightarrow gel \rightarrow liquid \rightarrow gel transitions. Qualitative observations of particle motion coincide with these slope changes. Excellent reversibility was observed in response to the reservoir fluid changes and the experiments underline that mass transport through the membrane was fast as a result of the small

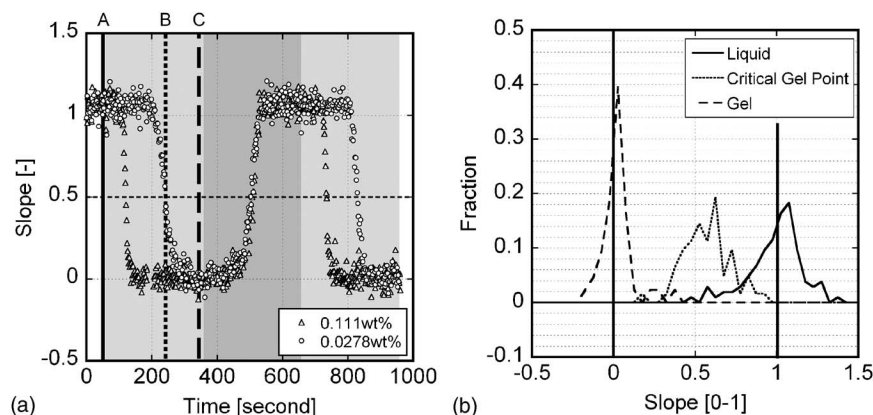


FIG. 8. (a) The transient slope at two different CaCl_2 concentrations: (\circ) 0.0278 wt. % and (\triangle) 0.111 wt. %. Solvents: (\square) NaCl, (light shaded area) CaCl_2 , and (dark shaded area) sodium citrate. (b) Histograms of $[\log(\text{MSD}) \text{ vs } \log(\tau)]$ slopes of individual particles at the three times marked in (a) for the 0.0278 wt. % sample.

sample dimensions. The slope and MSDs reached a saturated value after each stepwise solvent change, indicating that the time intervals in Table II were appropriate to capture the full rheological transition.

The concentration profiles of all three solutes (NaCl, CaCl_2 , and sodium citrate) were also determined through numerical calculations and are presented in Fig. 7(c). Comparison between Figs. 7(a)–7(c) shows that there are subtleties in the relation between rheological transitions and solute concentrations. These details are related to the kinetics of gel formation and can be emphasized by performing experiments at different solute concentrations. Figure 8(a) shows the response curves for two experiments with different CaCl_2 concentrations. As the CaCl_2 concentration in the reservoir flow increases, the liquid-to-gel transition occurs more rapidly; the more calcium is supplied to the sample, the faster the alginate gel is expected to form. Gel break-up, on the other hand, is delayed by increasing the CaCl_2 concentration; at higher CaCl_2 concentrations more Ca^{2+} ions must be chelated by incoming citrate to achieve gel break-up. Citrate ions are initially consumed by free Ca^{2+} ions in solution, before reaction with calcium ions in the gel can occur. It is clear that the response curves are very sensitive to the balance between reactants.

The dotted lines in Figs. 7(b) and 8(a) denote the occurrence of slope=0.5 in the MSD- τ -plot, which we chose to represent the gel point. A widely accepted definition of the critical gel point is a concentration at which $G' \sim G'' \sim \omega^{0.5}$, G' and G'' being the storage modulus and loss modulus and ω the angular frequency [Winter and Chambon (1986)]. The relation $G' \sim G'' \sim \omega^{0.5}$ reduces to $\langle \Delta r^2(\tau) \rangle \sim \tau^{0.5}$ for microrheological measurements, which in turn corresponds to slope=0.5 in a double-logarithmic plot of MSD versus τ [Figs. 7(b) and 8(a)].

The gelation experiments were repeated at different locations in the sample chamber between the membrane and the bottom of the chamber. The gelation times after switching the fluid flow were determined at each location (not shown here) and found to increase for larger distances to the membrane. The lag time at the top of the sample chamber was approximately 10 s longer than at the bottom, which is in good agreement with the predictions from numerical calculations [Fig. 2(b)]. The dialysis cell enables tracking of the gelation front by varying the location of the focal plane of the microscope.

To investigate the homogeneity of the sample during gelation, the MSDs of individual

particles were determined for three time intervals of 15 s [Fig. 8(a)]: in the liquid state, around the ensemble averaged gel point, and in the gel state. For each particle, a linear fit in a double-logarithmic plot of MSD vs τ was used to extract the slope and Fig. 8(b) shows the histograms of the slope distributions during the three intervals. In the liquid and gel state, clear peaks were observed around 0 and 1, the expected values for liquid-like and gellike samples (see also Fig. 6). For homogeneous samples, one would expect to find narrow peaks. However, the finite width of the peaks in Fig. 8(b) should not be attributed to heterogeneity, but is the result of insufficient statistical information to accurately determine the slope for individual particles. This conclusion is supported by the occurrence of unphysical negative slope values in the gel state. The most significant result in Fig. 8(b) is the slope distribution at the gelation point. If gelation would have occurred heterogeneously, one would expect to see a very broad distribution of slopes, some particles being in a liquid environment (slope 1) and others embedded in an elastic gel (slope 0). Instead, the middle peak in Fig. 8(b) has a width that is similar to the distribution in the liquid state. Therefore, it can be concluded that no significant heterogeneity occurred within the field of view during gelation.

The transient experiments and trajectory analysis on the alginate samples illustrate that the dialysis cell with particle tracking microrheology is a powerful tool for monitoring sample rheology in response to solvent changes. The device enables accurate and quantitative measurements of liquid-to-gel transitions, tracking the progression of the gel front, and detecting (in)homogeneity of the sample. The determination of transient rheological properties makes it possible to investigate the dynamics of complex fluids in ways that would be impossible with macrorheological measurements on a rheometer.

B. Sodium polystyrene sulfonate, NaPSS


Sodium polystyrene sulfonate is a polyelectrolyte, which in aqueous solution is highly salt-sensitive, because Coulombic repulsion between charged monomers plays a major role in the polymer conformation. The viscosity of aqueous solutions dramatically drops upon the addition of salt, e.g., KBr and NaCl [Fuoss and Strauss (1948); Boris and Colby (1998)], due to the screening of intra- and intermolecular electrostatic interactions. The steady shear viscosity of NaPSS has been reported in literature; at low shear rates, NaPSS solutions were found to exhibit Newtonian behavior both before and after the addition of salt [Boris and Colby (1998)]. We chose this polyelectrolyte for further exploration of the capabilities of the dialysis cell.

A stock solution of 10 wt. % NaPSS (M_w 1 200 000, #628, Scientific Polymer Product Inc.) was prepared in a vial and mixed well with DI-water on a vortex mixer. After leaving the sample for 48 h, the stock solution was diluted with DI-water and fluorescent probe particles were added, so that a 5 wt. % NaPSS solution was obtained. The surface of carboxylate modified fluorescent polystyrene particles (F8819, 1 μm diameter, IDC) was modified with polyethylene glycol (PEG) [Kim *et al.* (2005)] in order to prevent particle aggregation due to interactions between the particles and NaPSS polymer chains. The particle size of the functionalized particles was calibrated in DI-water and the average particle diameter was 1.03 μm .

Analogous to the sodium alginate experiments, we performed reversibility experiments. Table III lists a typical program of solvent manipulation. The reservoir flow started with 0.1 M NaCl, was switched to 1 M NaCl, and then switched back to 0.1 M NaCl.

Transient response curves for five different τ values with interval length $\Delta t = 3$ s are shown in Fig. 9(a). The MSD increased with the addition of salt and decreased when the

TABLE III. Composition of the reservoir flow during NaPSS experiments.

Switching time		Interval (min)	Reservoir flow
0		1	0.1 M NaCl
1		5	1 M NaCl
6		5	0.1 M NaCl
11			

sample was dialyzed at low salt concentration. The observed reversibility again proves the selectivity of the membrane as discussed in Sec. IV A for alginate. The time intervals of the solvent exchange were chosen so that the MSD reached a plateau region in each interval. The MSD increased with τ in all solvents, which indicates that the samples exhibited liquidlike behavior at all NaCl concentrations. For liquidlike samples, the viscosity can be obtained from the Stokes-Einstein equation, $\langle \Delta r^2(\tau) \rangle = 2dD\tau$, where $D = k_B T / 6\pi\eta a$, d is the dimensionality of the displacement vector Δr , a is the tracer particle

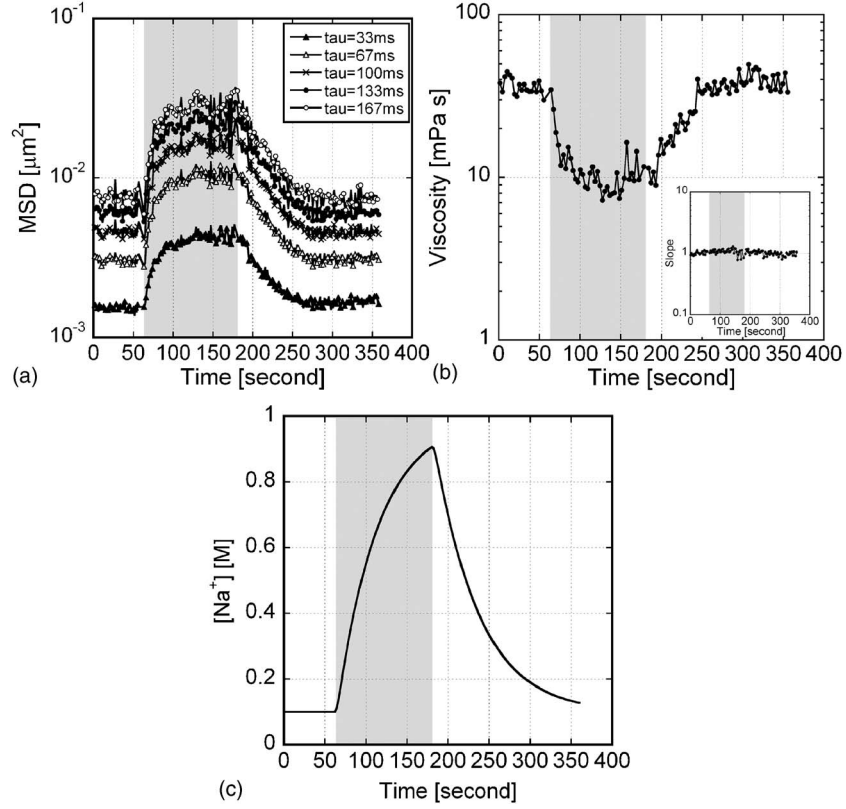


FIG. 9. (a) Transient MSD of NaPSS at different NaCl concentrations. τ =(\blacktriangle) 33 ms, (\triangle) 67 ms, (\times) 100 ms, (\bullet) 133 ms, and (\circ) 167 ms. Solvents: (light shaded area) 0.1 M NaCl and (dark shaded area) 1 M NaCl. (b) Transient viscosity. (c) Numerical calculations of solvent composition.

radius, and η is the solvent viscosity. The resulting transient viscosity curve is shown in Fig. 9(b). A rapid response of viscosity to solvent change was observed. The inset in Fig. 9(b) shows the slope of the MSD- τ -plot as a function of time and confirms that the sample behaved like a Newtonian fluid at all times.

To confirm that the viscosity response yields quantitatively correct values, steady state microrheology experiments were performed (see Sec. IV A for details). Stock solutions of 10 wt. % sodium alginate in 0.2 M and 2 M NaCl were prepared and mixed in different vials. After leaving them for 48 h, the stock solutions were diluted with DI-water and fluorescent probe particles, so that 5 wt. % NaPSS solutions in respectively 0.1 M and 1 M NaCl were obtained. The microrheological viscosities of the sample were found to be 37.5 mPa s and for 1 M NaCl solution and 14.1 mPa s for 1 M NaCl solution. As mentioned previously, the deviation from the viscosity found in transient experiments originates from the difference in sample treatment: in the dialysis cell, the sample is in continuous contact with a solvent stream of constant composition. Viscosity measurements were also performed on a controlled stress rheometer (see Sec. IV A). The rheometer data showed Newtonian behavior for both samples in the low shear region, and zero-shear viscosities of, respectively, 37.1 mPa s and 13.5 mPa s, in excellent agreement with steady state microrheology. These results prove that microrheology yields bulk rheological properties for NaPSS solutions and that transient microrheology can be used to quantitatively capture the changes of sample rheology.

V. CONCLUSION

A new dialysis cell for microrheology was constructed by integrating particle tracking microrheology and microfluidics. The device enables quantitative measurements of the transient rheological response of complex fluids to changes in solvent composition. Such experiments are not possible in a traditional mechanical rheometer. We characterized the diffusion process in the dialysis cell both experimentally and numerically, and were able to manipulate solvent composition in a controlled and predictable fashion with a characteristic response time of a few minutes. In future designs, we plan to shorten the diffusive time scale even further by using shorter diffusion paths. As an example of applications for this new device, we successfully quantified the transient rheological responses of the liquid-gel transition of sodium alginate hydrogels in the presence of multivalent cations and the changes in viscosity of NaPSS solutions as a result of variations in ionic strength. This study introduces a new paradigm for microrheological studies that is applicable to a wide variety of solvent-responsive complex fluids.

ACKNOWLEDGMENTS

The authors are grateful to Dr. Athanasios Nenes for providing the FVM simulation code and Dr. Clifford L. Henderson and Travis Anderson for their help with microfabrication. The authors also thank Dr. Eric Weeks and Dr. Denis Semwogerere at Emory University for their assistance with confocal microscopy. The work was supported by the Petroleum Research Fund of the American Chemical Society (ACS-PRF) Grant No. 41208-G9 and by the Georgia Tech Research Foundation.

References

- Beebe, D. J., J. S. Moore, J. M. Bauer, Q. Yu, R. H. Liu, C. Devadoss, and B. H. Jo, "Functional hydrogel structures for autonomous flow control inside microfluidic channels," *Nature (London)* **404**, 588–590 (2000).
- Boris, D. C., and R. H. Colby, "Rheology of sulfonated polystyrene solutions," *Macromolecules* **31**, 5746–5755 (1998).
- Bowen, W. R., N. Hilal, R. W. Lovitt, and P. M. Williams, "Atomic force microscope studies of membranes: Surface pore structures of cyclopore and anopore membranes," *J. Membr. Sci.* **110**, 233–238 (1996).
- Brannonpeppas, L., and N. A. Peppas, "Dynamic and equilibrium swelling behavior of pH-sensitive hydrogels containing 2-hydroxyethyl methacrylate," *Biomaterials* **11**, 635–644 (1990).
- Brannonpeppas, L., and N. A. Peppas, "Time-dependent response of ionic polymer networks to pH and ionic-strength changes," *Int. J. Pharm.* **70**, 53–57 (1991).
- Breedveld, V., and D. J. Pine, "Microrheology as a tool for high-throughput screening," *J. Mater. Sci.* **38**, 4461–4470 (2003).
- Chen, G. P., Y. Imanishi, and Y. Ito, "Photolithographic synthesis of hydrogels," *Macromolecules* **31**, 4379–4381 (1998).
- Crocker, J. C., and D. G. Grier, "Methods of digital video microscopy for colloidal studies," *J. Colloid Interface Sci.* **179**, 298–310 (1996).
- deBeer, D., P. Stoodley, and Z. Lewandowski, "Measurement of local diffusion coefficients in biofilms by microinjection and confocal microscopy," *Biotechnol. Bioeng.* **53**, 151–158 (1997).
- Deen, W. M., "Hindered transport of large molecules in liquid-filled pores," *AIChE J.* **33**, 1409–1425 (1987).
- Fuoss, R. M., and U. P. Strauss, "Electrostatic interaction of polyelectrolytes and simple electrolytes," *J. Polym. Sci.* **3**, 602–603 (1948).
- Goeden-Wood, N. L., J. D. Keasling, and S. J. Muller, "Self-assembly of a designed protein polymer into beta-sheet fibrils and responsive gels," *Macromolecules* **36**, 2932–2938 (2003).
- Gondret, P., N. Rakotomalala, M. Rabaud, D. Salin, and P. Watzky, "Viscous parallel flows in finite aspect ratio hele-shaw cell: Analytical and numerical results," *Phys. Fluids* **9**, 1841–1843 (1997).
- Grant, G. T., E. R. Morris, D. A. Rees, P. J. C. Smith, and D. Thom, "Biological interactions between polysaccharides and divalent cations—egg box model," *FEBS Lett.* **32**, 195–198 (1973).
- Gupta, P., K. Vermani, and S. Garg, "Hydrogels: From controlled release to pH-responsive drug delivery," *Drug Discovery Today* **7**, 569–579 (2002).
- Hassan, C. M., F. J. Doyle, and N. A. Peppas, "Dynamic behavior of glucose-responsive poly(methacrylic acid-g-ethylene glycol) hydrogels," *Macromolecules* **30**, 6166–6173 (1997).
- Hernandez, A., F. Martinez, A. Martin, and P. Pradanos, "Porous structure and surface-charge density on the walls of microporous alumina membranes," *J. Colloid Interface Sci.* **173**, 284–296 (1995).
- Hernandez, A., J. I. Calvo, P. Pradanos, L. Palacio, M. L. Rodriguez, and J. A. de Saja, "Surface structure of microporous membranes by computerized sem image analysis applied to anopore filters," *J. Membr. Sci.* **137**, 89–97 (1997).
- Hines, Anthony L., and Robert N. Maddox, *Mass Transfer: Fundamentals and Applications* (Prentice-Hall, Englewood Cliffs, NJ, 1984).
- Hoffman, A. S., "Intelligent polymers in medicine and biotechnology," *Macromol. Symp.* **98**, 645–664 (1995).
- Hou, L., K. Lubyphelps, and F. Lanni, "Brownian-motion of inert tracer macromolecules in polymerized and spontaneously bundled mixtures of actin and filamin," *J. Cell Biol.* **110**, 1645–1654 (1990).
- Jeong, B., and A. Gutowska, "Lessons from nature: Stimuli-responsive polymers and their biomedical applications (vol 20, pg 305, 2002)," *Trends Biotechnol.* **20**, 360–360 (2002).
- Keller, M., J. Schilling, and E. Sackmann, "Oscillatory magnetic bead rheometer for complex fluid microrheometry," *Rev. Sci. Instrum.* **72**, 3626–3634 (2001).
- Kim, A. J., V. N. Manoharan, and J. C. Crocker, "Swelling-based method for preparing stable, functionalized polymer colloids," *J. Am. Chem. Soc.* **127**, 1592–1593 (2005).
- Kim, B., K. La Flamme, and N. A. Peppas, "Dynamic swelling behavior of pH-sensitive anionic hydrogels used for protein delivery," *J. Appl. Polym. Sci.* **89**, 1606–1613 (2003).

- Larson, Ronald G., *The Structure and Rheology of Complex Fluids* (Oxford University Press, New York, 1999).
- Lide, D. R., *CRC Handbook of Chemistry and Physics* (CRC Press, Boca Raton, Florida, 2003).
- Mason, T. G., and D. A. Weitz, "Optical measurements of frequency-dependent linear viscoelastic moduli of complex fluids," *Phys. Rev. Lett.* **74**, 1250–1253 (1995).
- Mason, T. G., K. Ganesan, J. H. vanZanten, D. Wirtz, and S. C. Kuo, "Particle tracking microrheology of complex fluids," *Phys. Rev. Lett.* **79**, 3282–3285 (1997).
- Mason, T. G., "Estimating the viscoelastic moduli of complex fluids using the generalized stokes-einstein equation," *Rheol. Acta* **39**, 371–378 (2000).
- Matsumoto, T., and K. Mashiko, "Viscoelastic properties of alginate aqueous-solutions in the presence of salts," *Biopolymers* **29**, 1707–1713 (1990).
- McGrath, J. J., "A microscope diffusion chamber for the determination of the equilibrium and non-equilibrium osmotic response of individual cells," *J. Microsc.* **139**, 249–263 (1985).
- McGrath, J. J., and S. Krings, "Computer-controlled concentration histories in a microscope diffusion chamber," *Cryobiology* **23**, 546–546 (1986).
- McGrath, J. J., "Quantitative measurement of cell membrane transport: Technology and applications," *Cryobiology* **34**, 315–334 (1997).
- Moaddeb, M., and W. J. Koros, "Gas transport properties of thin polymeric membranes in the presence of silicon dioxide particles," *J. Membr. Sci.* **125**, 143–163 (1997).
- Montermini, D., C. P. Winlove, and C. C. Michel, "Effects of perfusion rate on permeability of frog and rat mesenteric microvessels to sodium fluorescein," *J. Physiol. (London)* **543**, 959–975 (2002).
- Palacio, L., P. Pradanos, J. I. Calvo, and A. Hernandez, "Porosity measurements by a gas penetration method and other techniques applied to membrane characterization," *Thin Solid Films* **348**, 22–29 (1999).
- Patankar, Suhas V., *Numerical Heat Transfer and Fluid Flow* (Hemisphere, New York, 1980).
- Peppas, N. A., P. Bures, W. Leobandung, and H. Ichikawa, "Hydrogels in pharmaceutical formulations," *Eur. J. Pharm. Biopharm.* **50**, 27–46 (2000).
- Porsche, A. M., C. Korber, S. Englich, U. Hartmann, and G. Rau, "Determination of the permeability of human-lymphocytes with a microscope diffusion chamber," *Cryobiology* **23**, 302–316 (1986).
- Qiu, Y., and K. Park, "Environment-sensitive hydrogels for drug delivery," *Adv. Drug Delivery Rev.* **53**, 321–339 (2001).
- Rudzinski, W. E., A. M. Dave, U. H. Vaishnav, S. G. Kumbar, A. R. Kulkarni, and T. M. Aminabhavi, "Hydrogels as controlled release devices in agriculture," *Des. Monomers Polym.* **5**, 39–65 (2002).
- Shirai, Y., K. Hashimoto, H. Yamaji, and M. Tokashiki, "Continuous production of monoclonal-antibody with immobilized hybridoma cells in an expanded bed fermenter," *Appl. Microbiol. Biotechnol.* **26**, 495–499 (1987).
- Siegel, R. A., I. Johannes, C. A. Hunt, and B. A. Firestone, "Buffer effects on swelling kinetics in polybasic gels," *Pharm. Res.* **9**, 76–81 (1992).
- Smidsrod, O., and G. Skjakbraek, "Alginate as immobilization matrix for cells," *Trends Biotechnol.* **8**, 71–78 (1990).
- Soppimath, K. S., T. M. Aminabhavi, A. M. Dave, S. G. Kumbar, and W. E. Rudzinski, "Stimulus-responsive Smart Hydrogels as novel drug delivery systems," *Drug Dev. Ind. Pharm.* **28**, 957–974 (2002).
- Stone, H. A., and S. Kim, "Microfluidics: Basic issues, applications, and challenges," *AIChE J.* **47**, 1250–1254 (2001).
- Tanaka, H., M. Matsumura, and I. A. Veliky, "Diffusion characteristics of substrates in caalginate gel beads," *Biotechnol. Bioeng.* **26**, 53–58 (1984).
- van der Linden, H. J., S. Herber, W. Olthuis, and P. Bergveld, "Stimulus-sensitive hydrogels and their applications in chemical (micro) analysis," *Analyst (Cambridge, U.K.)* **128**, 325–331 (2003).
- Wang, Z. Y., Q. Z. Zhang, M. Konno, and S. Saito, "Sol-gel transition of alginate solution by additions of various divalent-cations—critical-behavior of relative viscosity," *Chem. Phys. Lett.* **186**, 463–466 (1991).
- Wang, Z. Y., Q. Z. Zhang, M. Konno, and S. Saito, "Sol-gel transition of alginate solution by the addition of various divalent-cations—a rheological study," *Biopolymers* **34**, 737–746 (1994).
- Winter, H. H., and F. Chambon, "Analysis of linear viscoelasticity of a cross-linking polymer at the gel point," *J. Rheol.* **30**, 367–382 (1986).